Extraction of Time-Varying Bridge Frequency from Responses of Two-Axle Vehicles

Zhenkun Li[1(✉)], Yifu Lan[1], Kun Feng[2], and Weiwei Lin[1]

[1] Department of Civil Engineering, Aalto University, 02150 Espoo, Finland
zhenkun.li@aalto.fi

[2] Faculty of Engineering, Agri-Tech and the Environment, Anglia Ruskin University, Peterborough, UK

Abstract. Bridge frequencies are important characteristics for its lifecycle condition assessment. The drive-by method, which only requires several sensors installed on the passing vehicle and employs vehicle responses to extract essential information about the bridge, has been a focus in the last two decades due to its low-cost and efficient nature. Such a method typically relies on the vehicle-bridge interaction and assumes that the bridge's frequency does not change during the vehicle passage. However, practical applications indicate that the bridge frequencies can change during the interaction process, especially when the vehicle mass is comparable to that of the bridge. This paper further investigates the time-varying frequency of the vehicle-bridge interaction system incorporating a two-axle vehicle and a simply supported bridge. Firstly, the semi-analytical solution for time-varying bridge frequency was developed and numerical simulations were performed to verify the solution. Different frequency and mass ratios between the vehicle and bridge were explored. Then, the approach to acquire clear time-frequency representations of the vehicle responses for bridge frequency extraction was presented, and ridge extraction was employed to extract the traces of time-varying bridge frequencies. Finally, laboratory experiments, including a scaled two-axle vehicle and a steel beam model, were conducted and the effectiveness of the proposed method for extracting time-varying bridge frequencies was demonstrated.

Keywords: Vehicle-bridge interaction · Bridge frequency · Drive-by · Time-varying

1 Introduction

Many bridges in Europe have been in service for quite many years. Recently, it has been discovered that some of these bridges are experiencing aging and deterioration, which could lead to potential failures if regular maintenance is not properly conducted. Therefore, monitoring the health condition of bridges has become crucial, and comprehensive reports on bridge assessments and residual life predictions are essential. Among various bridge assessment methods, vibration-based approaches have proven to be promising and effective for indicating the health condition of bridges. Over the past decades, the

Á. Cunha and E. Caetano (Eds.): EVACES 2025, LNCE 676, pp. 300–310, 2025.
https://doi.org/10.1007/978-3-031-96114-4_32

dynamic characteristics of bridges have been utilized as reliable damage indicators [1, 2].

Among all dynamic characteristics, the natural frequency (referred to as "frequency" in this paper) of a bridge is one of the most fundamental and important indicators, as it can be used to detect the presence of damage [3]. Traditionally, obtaining the bridge's frequencies requires engineers to install sensors on the structure. However, with the growing demand for labor and the increasing number of newly constructed bridges, this method has become both time-consuming and costly [4]. Therefore, there is a need for new, efficient, and cost-effective technologies to regularly monitor bridge conditions based on their frequencies.

In 2004, Yang et al. [5] proposed the indirect method, successfully identifying bridge frequencies using a spring-mass-modeled vehicle. This study laid the foundation for further developments in identifying bridge modal shapes and damping ratios through vehicle responses [6, 7], as well as in damage detection [8–10]. The identification of bridge frequencies from vehicle responses has been extensively studied. Researchers have employed vehicles with modified parameters [11, 12], analyzed residual responses from connected vehicles [13, 14], and utilized contact-point responses [15, 16]. These methods have effectively minimized the influence of vehicle dynamics and road roughness. However, it is important to note that the indirect method heavily relies on vehicle-bridge interaction (VBI). Most studies have assumed that vehicles do not cause significant variations in bridge frequencies. Recent research has demonstrated that heavy vehicles can enhance the transfer of bridge information to vehicle vibrations [17, 18]. However, heavy vehicle traffic can introduce variability in bridge frequencies, potentially masking frequency changes caused by bridge damage. Therefore, when heavy vehicles are used, researchers should focus on analyzing time-varying bridge frequencies rather than relying solely on frequencies identified from the vehicle response spectrum.

Time-frequency analysis provides crucial insights for examining non-stationary signals. In 2017, Cantero et al. [19] observed the evolution of bridge frequencies and vibration modes during truck passages in field tests. However, traditional methods such as the short-time Fourier transform (STFT) and wavelet transform (WT) often suffer from blurred time-frequency representations (TFRs), making it difficult to clearly capture variations in bridge frequencies. In 2013, Yang et al. [20] analytically derived the analytical frequency evolution of a VBI system modeled with a spring-mass and a simply supported beam. Later, in 2020, Li et al. [21] successfully identified the clear time-varying characteristics of bridge frequencies from vehicle responses using the synchroextracting transform. In 2023, Tan et al. [22] extracted time-varying bridge frequencies from drive-by vehicle vibrations in a laboratory experiment, developing an adaptive second-order synchrosqueezing transform. In the same year, He et al. [23] explored the identification of higher-order modal frequencies of bridges using the synchrosqueezing transform, validating the method through numerical simulations and experiments. Despite these advancements, existing studies have typically relied on simple spring-mass models, with limited consideration of vehicle pitching effects. Additionally, recent research has revealed that high-order synchrosqueezing transform methods are highly sensitive to noise, often producing unsatisfactory results when applied to signals with significant noise interference.

This paper explores the evolution of bridge frequencies when a two-axle vehicle passes over a bridge. First, a new semi-analytical solution is developed to describe the time-varying frequencies of the VBI system, which includes a two-axle vehicle and a simply support bridge. Next, the frequency amplification ratios of the system are analyzed under varying vehicle-bridge frequency and mass ratios. Additionally, an enhanced algorithm, the improved multisynchrosqueezing transform (IMSST), is employed to generate clear TFRs, and ridge extraction is used to trace the time-varying bridge frequencies. Finally, laboratory experiments using a scaled two-axle vehicle and a steel beam model are conducted to demonstrate the effectiveness of the proposed method for extracting time-varying bridge frequencies. The remainder of this paper is organized as follows: Sect. 2 presents the semi-analytical solutions for time-varying bridge frequencies and the fundamental theories for extracting the bridge's instantaneous frequencies (IFs) from vehicle responses. Section 3 explores the effects of vehicle-bridge frequency and mass ratios on bridge frequency amplification. Section 4 provides experimental validation using a scaled truck and a steel beam. Finally, the paper is concluded in Sect. 5.

2 Theories

In this paper, the vehicle is modeled as a single mass m_v, supported by two springs with stiffness values k_1 and k_2. The vehicle's moment of inertia is denoted by J_v. The axle distance is represented by a, with the center of gravity defined by a_1 and a_2. . The vehicle exhibits two degrees of freedom (DOFs): vertical displacement of the body (z_v) and body rotation (θ_v), as illustrated in Fig. 1. The bridge is modeled as a simply supported Euler–Bernoulli beam, characterized by a length L, flexural stiffness EI, and mass per unit length $\overline{m}$. For the analytical derivation, the influences of road roughness and damping are not included.

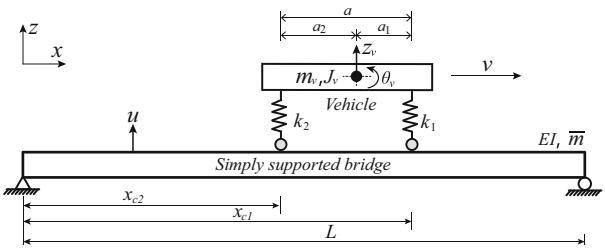

Fig. 1. Analytical model of the two-axle vehicle and bridge

The equilibrium equations for vibrations of the bridge and two-axle vehicle can be denoted by Eqs. (1), 2 and (3),

$$\overline{mu}(x,t) + EIu(x,t)'''' = \sum\nolimits_{i=1}^{2} f_{ci}(t)\delta(x - x_{ci}) \tag{1}$$

$$m_v\ddot{z}_v + k_1(z_v + a_1\theta_v - u_{c1}) + k_2(z_v - a_2\theta_v - u_{c2}) = 0 \tag{2}$$

$$J_v\overline{\theta}_v + k_1a_1(z_v + a_1\theta_v - u_{c1}) - k_2a_2(z_v - a_2\theta_v - u_{c2}) = 0 \tag{3}$$

where $u(x, t)$ denotes the deflection of the bridge. The notation $(\dot{})$ indicates differentiation with respect to time t, while $(')$ represents differentiation with respect to the bridge position x. The term $\delta(\cdot)$ refers to the Dirac delta function. The contact force between the vehicle and the bridge is denoted by $f_{ci}(t)$, which can be expressed as $f_{ci}(t) = k_i(z_{vi} - u_{ci}) - m_{vi}g$ and $z_{vi} = z_v + (-1)^{i+1}\theta_v a_i$, $i = 1, 2$. Here, z_{vi} is the i-th axle's displacement, and $m_{vi}g = m_v g(a - a_i)/a$ is the axle weight. g Represents the acceleration due to gravity. u_{ci} Denotes the deflection of the beam at the i-th contact point. The vertical deflection of the beam can be expressed using modal superposition. For simplicity, only the first mode of the beam is considered in analytical solutions. The beam's deflection can be represented as

$$u(x, t) = q_b(t)\sin(\pi x/L) \tag{4}$$

where $q_b(t)$ is the generalized coordinate (with t omitted for simplification in later steps). While higher modes of the beam can be included, they primarily increase mathematical complexity without significantly enhancing the understanding of the physical behavior [20]. In contrast, incorporating additional DOFs for the vehicle is valuable, as it aids in comprehending physical phenomena relevant to practical engineering applications. By substituting Eq. Into Eq., we obtain

$$\overline{m}\sin\Big(\frac{\pi x}{L}\Big)\ddot{q}_b + \frac{EI\pi^4}{L^4}\sin\Big(\frac{\pi x}{L}\Big)q_b = \sum_{i=1}^{2}\Big[k_i\Big(z_{vi} - \sin\Big(\frac{\pi x_{ci}}{L}\Big)q_b\Big) - m_{vi}g\Big]\delta(x - x_{ci}) \tag{5}$$

Note that the Dirac delta function appears in Eq. (5). It is multiplied by the mode $\sin(\pi x/L)$ and integrated with respect to x from 0 to L. After rearranging all terms related to $\ddot{q}_b$, q_b, z_v, and θ_v, we obtain

$$\begin{aligned}\Big[\frac{\overline{m}L}{2}\Big]\ddot{q}_b + \Big[\frac{EI\pi^4}{2L^3} + \sum_{i=1}^{2}k_i\sin^2\big(\frac{\pi x_{ci}}{L}\big)\Big]q_b - \Big[\sum_{i=1}^{2}k_i\sin\big(\frac{\pi x_{ci}}{L}\big)\Big]z_v \\ -\Big[\sum_{i=1}^{2}(-1)^{i+1}k_ia_i\sin\big(\frac{\pi x_{ci}}{L}\big)\Big]\theta_v = -\sum_{i=1}^{2}m_{vi}g\sin\big(\frac{\pi x_{ci}}{L}\big)\end{aligned} \tag{6}$$

By substituting Eq. (4) into Eqs. (2) and (3), we obtain

$$m_v\ddot{z}_v - \Big[\sum_{i=1}^{2}k_i\sin\Big(\frac{\pi x_{ci}}{L}\Big)\Big]q_b + (k_1 + k_2)z_v + (k_1a_1 - k_2a_2)\theta_v = 0 \tag{7}$$

$$J_v\ddot{\theta}_v - \Big[\sum_{i=1}^{2}(-1)^{i+1}k_ia_i\sin\Big(\frac{\pi x_{ci}}{L}\Big)\Big]q_b + (k_1a_1 - k_2a_2)z_v + \Big(k_1a_1^2 + k_2a_2^2\Big)\theta_v = 0 \tag{8}$$

Equations (6), (7), and (8) can be organized into a matrix form, as presented in Eq. (9)

$$\mathbf{M}_s[\ddot{q}_b, \ddot{z}_v, \ddot{\theta}_v]^T + \mathbf{K}_s\big[q_b, z_v, \theta_v\big]^T = \mathbf{f}_s \tag{9}$$

where $\mathbf{M}_s$, $\mathbf{K}_s$ represent the mass and stiffness matrices of the VBI system, respectively, and the vector $\mathbf{f}_s$ denotes the applied forces. The components of these matrices and the force vector are detailed in Eqs. (10) and (11).

$$\mathbf{M}_s = \begin{bmatrix} \frac{\overline{m}L}{2} & 0 & 0 \\ 0 & m_v & 0 \\ 0 & 0 & J_v \end{bmatrix}, \mathbf{f}_s = \left[-\sum_{i=1}^{2} m_{vi} g \sin\left(\frac{\pi x_{ci}}{L}\right), 0, 0 \right]^T \tag{10}$$

$$\mathbf{K}_s = \begin{bmatrix} \frac{EI\pi^4}{2L^3} + \sum_{i=1}^{2} k_i \sin^2\left(\frac{\pi x_{ci}}{L}\right) & -\sum_{i=1}^{2} k_i \sin\left(\frac{\pi x_{ci}}{L}\right) & -\sum_{i=1}^{2} (-1)^{i+1} k_i a_i \sin\left(\frac{\pi x_{ci}}{L}\right) \\ -\sum_{i=1}^{2} k_i \sin\left(\frac{\pi x_{ci}}{L}\right) & k_1 + k_2 & k_1 a_1 - k_2 a_2 \\ -\sum_{i=1}^{2} (-1)^{i+1} k_i a_i \sin\left(\frac{\pi x_{ci}}{L}\right) & k_1 a_1 - k_2 a_2 & k_1 a_1^2 + k_2 a_2^2 \end{bmatrix} \tag{11}$$

The equations presented above account for the interaction between the two-axle vehicle and the bridge. It is important to note that the stiffness matrix of the VBI system varies over time as the vehicle moves across the bridge. As a result, the frequencies of both the bridge and vehicle will vary. When the vehicle and bridge are considered separately, without interaction, each retains its original frequencies. The fundamental frequency of the bridge, in isolation, can be determined by $\omega_{b1,0} = \pi^2/L^2\sqrt{EI/\overline{m}}$. For the vehicle, the original vertical and pitching frequencies [24] are presented in Eq. (12),

$$\omega_{v0,p0}^2 = \frac{1}{2}\left(\frac{k_1 + k_2}{m_v} + \frac{k_1 a_1^2 + k_2 a_2^2}{J_v} \pm \sqrt{\left(\frac{k_1 + k_2}{m_v} - \frac{k_1 a_1^2 + k_2 a_2^2}{J_v} \right)^2 + \frac{4(k_1 a_1 - k_2 a_2)^2}{m_v J_v}} \right) \tag{12}$$

where $\omega_{v0,p0}$ represent the original vertical and pitching frequencies of the vehicle without interaction with the bridge. During the interaction between the vehicle and the bridge, the system's time-varying frequencies can be determined by solving the eigenvalue problem presented in Eq. (13).

$$\det\left(\mathbf{K}_s - \omega^2 \mathbf{M}_s\right) = 0 \tag{13}$$

Let $\Omega = \omega^2$, $\Omega > 0$. It can be observed that Eq. (13) is a cubic equation in terms of Ω. An efficient approach to find its solution is to find the numerical roots when all other parameters are known except Ω. Since $\mathbf{K}_s$ and $\mathbf{M}_s$ consist of real numbers and are both symmetric and positive definite, Ω will always yield real and positive solutions. Consequently, the time-varying frequencies of the VBI system, ω_{b1}, ω_v, and ω_p, can be determined by $\omega = \sqrt{\Omega}$ as the vehicle moves across different positions on the bridge. Then, the IMSST algorithm [25, 26] was adopted to generate TFRs of the vehicle's vibrations, which is more concentrated than that generated by the traditional algorithms, such as STFT and WT. Then, a popular multi-ridge extraction algorithm [27, 28] is employed to extract IFs of the VBI system.

3 Effects of Vehicle-Bridge Frequency and Mass Ratios

After the analytical solution is obtained in the last section, in this section, the effects of vehicle-bridge frequency and mass ratios on bridge frequency amplification are investigated. In the following content, the frequency (f) expressed in Hz is utilized instead

of the circular frequency (ω) in rad/s. Here, $f_{b1}^0 = \omega_{b1,0}/2\pi$, and $f_{v,p}^0 = \omega_{v0,p0}/2\pi$. The shared parameters for all vehicles are as follows: $J_v = 700\ \text{kg} \cdot \text{m}^2$, $a_1 = 0.5$ m, $a_2 = 1.5$ m. For the bridge, it is divided into 50 elements, with the following parameters: $L = 25$ m, $E = 27.5$ GPa, $I = 0.15\ \text{m}^4$, and $\overline{m} = 2000$ kg/m. With these parameters, the original frequencies of the bridge without interaction with vehicles can be calculated as $f_{b1}^0 = 3.609$ Hz, $f_{b2}^0 = 14.438$ Hz, $f_{b3}^0 = 32.485$ Hz. Damping effects and road roughness are temporarily ignored for theoretical validations in this section. Then, $m_v/\overline{m}L$ is modified from 0.01 to 0.5 with an increment of 0.01, and the frequency ratio f_v^0/f_{b1}^0 varies from 0.05 to 2 with an interval of 0.05. Figure 2 has shown the bridge frequency amplification ratio.

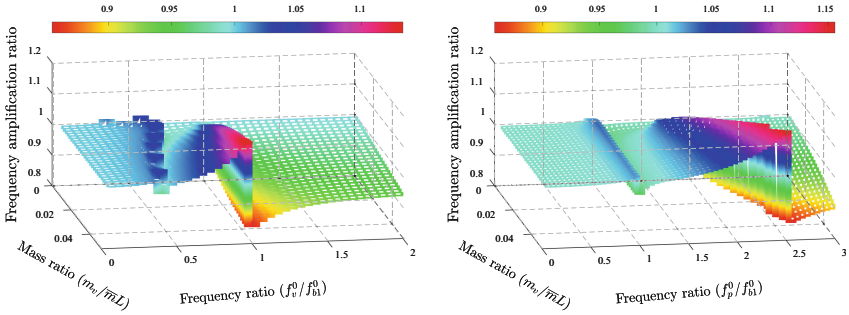

(a) x-axis is f_v^0/f_{b1}^0 (b) x-axis is f_p^0/f_{b1}^0

Fig. 2. Analytical model of the two-axle vehicle and bridge.

As can be seen, Fig. 2 illustrates the maximum frequency amplification ratios of f_{b1}, specifically when the vehicle's center of gravity crosses the midpoint of the bridge. Two different x-axes are used to depict the amplification effects. Figure 2a shows that as the ratio f_v^0/f_{b1}^0 increases, distinct frequency amplification peaks and valleys begin to appear when the ratio approaches 0.4. In comparison, Fig. 2b reveals that even when f_v^0/f_{b1}^0 is less than 1.0, f_p^0/f_{b1}^0 approaches 1.0, leading to low-peak frequency amplifications. Furthermore, these low peaks and valleys exhibit minimal sensitivity to mass ratios. As f_v^0/f_{b1}^0 continues to increase in Fig. 2a, it becomes evident that the most significant peaks and valleys occur around a f_v^0/f_{b1}^0 ratio of 1.0. At this point, f_p^0/f_{b1}^0 rises steadily from 1.5 to 2.5. Additionally, the mass ratio has a notable effect on frequency amplification, with lower vehicle-bridge mass ratios showing relatively limited influence. Based on this analysis, it can be concluded that the resonance between the vehicle's vertical frequency and f_{b1} significantly affects the bridge's fundamental frequency. However, the vehicle's pitching frequency also induces notable frequency amplification in f_{b1}, even when the mass ratio has a minimal impact on the amplification. In the following section, in order to clearly see the frequency amplification, a relatively heavy vehicle is employed in this paper.

4 Experimental Validation

4.1 Experimental Setups

In the laboratory experiments, a scaled truck and a steel beam are utilized to simulate the VBI system. Figure 3a has depicted the experimental setup overview. The vehicle's mass is 5.357 kg. One accelerometer is installed on the vehicle's body, as shown in Fig. 3b. Note that the vehicle's speed may change a little during the passage but is kept around 0.11 m/s. The truck's first two frequencies f_{v1}^0 and f_{v2}^0 are obtained as 19.708 Hz and 43.528 Hz. For the bridge, it is simulated by a beam shown in Fig. 3a. The beam's length is 6.0 m, and 0.15 m is reserved for each end. The beam's mass is 248.64 kg, making the vehicle-bridge mass ratio 2.155%. Two accelerometers are installed on the 1/3 span of the bridge to collect its vibrations. With impulse impact excitation, the beam's first three frequencies, f_{b1}^0, f_{b2}^0, and f_{b3}^0 are obtained as 7.499, 28.997, and 49.095 Hz.

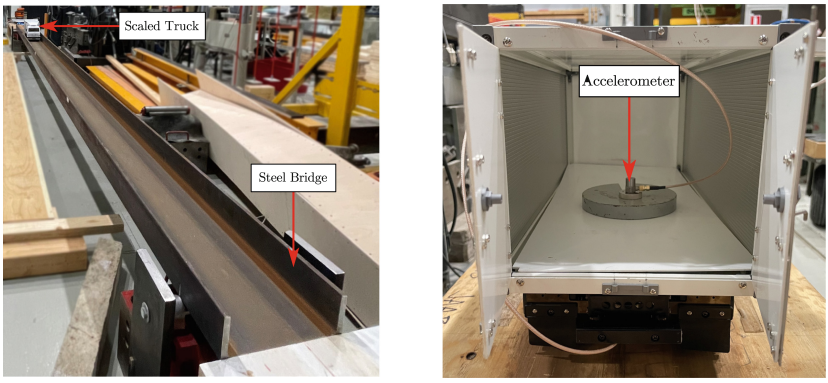

(a) Experimental overview (b) Truck

Fig. 3. Experimental setup.

4.2 Results and Discussions

When the truck moves on the beam, the frequency spectrum of the vehicle's body is shown in Fig. 4a. It reveals that the bridge's first two natural frequencies can be identified. However, it is important to note that the results obtained through direct Fast Fourier Transform (FFT) do not capture the time-varying characteristics of the VBI system. To address this, the IMSST is employed to analyze the vibrations of both the vehicle body and the bridge, as illustrated in Fig. 4b and c. The window length for the IMSST is set to 12288. From the direct measurement of the bridge vibrations, it is clearly observed that the bridge's fundamental frequency decreases as the vehicle passes over it, while the variation in the second frequency is less pronounced. Additionally, the decrease in the bridge's fundamental frequency is also detectable in the vehicle's responses, as shown in Fig. 4c.

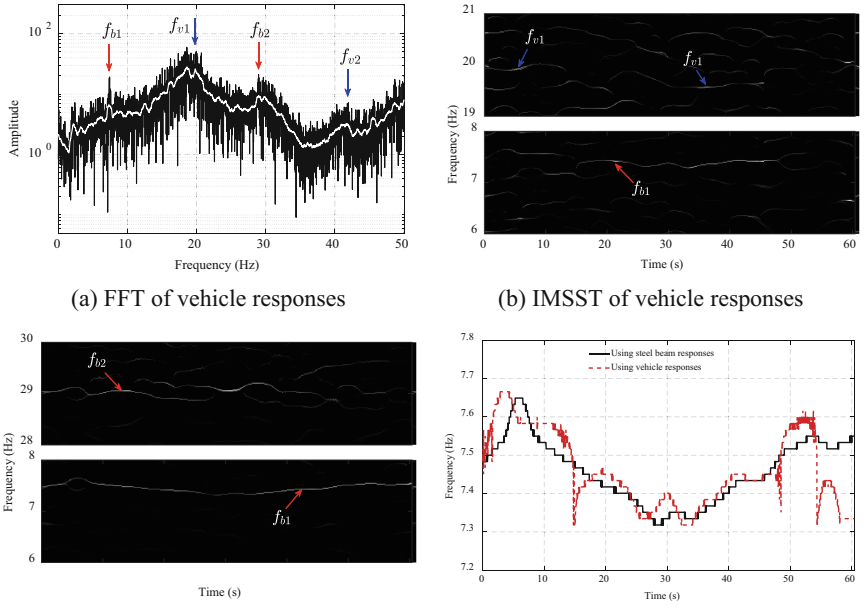

(a) FFT of vehicle responses

(b) IMSST of vehicle responses

(c) IMSST of bridge responses

(d) Extracted IFs from the vehicle and bridge

Fig. 4. Time-varying bridge frequency identification results.

The ridge extraction results for the bridge's fundamental frequency (f_{b1}) from the TFRs of both the vehicle and bridge responses are presented in Fig. 4d. These results demonstrate that the time-varying frequency of the bridge during the VBI process can be accurately captured by the drive-by vehicle. However, when the vehicle enters or exits the bridge, the fundamental frequency of the bridge is not as effectively captured. This is because the vehicle starts to collect bridge vibration data only upon entering the bridge and ceases to do so once it leaves.

5 Conclusions and Future Studies

In this paper, the time-varying frequencies of a bridge subjected to a moving two-axle vehicle are investigated. Novel semi-analytical solutions for the VBI system are derived. Using these solutions, the amplification of bridge frequencies is analyzed concerning the vehicle-bridge frequency and mass ratios. Subsequently, in laboratory experiments, the IMSST is employed to produce clear TFRs of the vibrations recorded from both the vehicle and the bridge. Based on these investigations, the following conclusions can be drawn:

1. The frequency amplification results, obtained under different vehicle-bridge frequency and mass ratios, clearly indicate that both the pitching and vertical frequencies of the vehicle influence the variation of the bridge's time-varying frequencies.

2. The effect of the vehicle's pitching frequency is less significant compared to that of the vertical frequency. Additionally, an increase in the vehicle's mass leads to greater amplification of the bridge's frequencies.
3. When the TFRs generated by IMSST are utilized, experimental results show that the extracted time-varying IFs from both the vehicle and bridge vibrations closely match. This well demonstrates the effectiveness of the presented indirect time-varying IF extraction approach.

Although the time-varying characteristics of the bridge were studied in this work, the influence of additional factors, such as multi-axle vehicles and heavy ongoing traffic, needs to be further investigated in future studies.

Acknowledgement. This research is financially sponsored by the Jane and Aatos Erkko Foundation in Finland (Decision number: 210018) and Aalto University (research project funding in ENG 2022). We acknowledge the provision of facilities and technical support in the Department of Civil Engineering and the Solid Mechanics Laboratory in the Department of Mechanical Engineering at Aalto University. The calculations presented above were partly performed using computer resources within the Aalto University School of Science "Science-IT" project.

References

1. Hou R, Xia Y (2021) Review on the new development of vibration-based damage identification for civil engineering structures: 2010–2019. J. Sound Vib. 491:115741. https://doi.org/10.1016/j.jsv.2020.115741
2. Li Z, Hou J, Jankowski Ł (2022) Structural damage identification based on estimated additional virtual masses and Bayesian theory. Struct. Multidiscip. Optim. 65(2):45. https://doi.org/10.1007/s00158-021-03156-y
3. Hou J, Li Z, Jankowski Ł, Wang S (2020) Estimation of virtual masses for structural damage identification. Struct. Control Health Monit. 27(8):e2585. https://doi.org/10.1002/stc.2585
4. Xu, H., et al.: Review of vehicle scanning method for bridges from 2004 to 2024. Int. J. Struct. Stab. Dyn. (2024). https://doi.org/10.1142/S0219455425300034
5. Yang YB, Lin CW, Yau JD (2004) Extracting bridge frequencies from the dynamic response of a passing vehicle. J. Sound Vib. 272(3–5):471–493. https://doi.org/10.1016/S0022-460X(03)00378-X
6. Zhang J, Yi T-H, Qu C-X, Han Q, Wang Y-F, Mei X-D (2023) Experimental studies of extracting bridge mode shapes by response of a moving vehicle. J. Bridge Eng. 28(11):4023076. https://doi.org/10.1061/JBENF2.BEENG-6243
7. Xu H, Liu YH, Chen J, Yang DS, Yang YB (2024) Novel formula for determining bridge damping ratio from two wheels of a scanning vehicle by wavelet transform. Mech. Syst. Signal Process. 208:111026. https://doi.org/10.1016/j.ymssp.2023.111026
8. Feng K, Casero M, González A (2023) Characterization of the road profile and the rotational stiffness of supports in a bridge based on axle accelerations of a crossing vehicle. Comput. Aided Civil Infrastruct. Eng. 38(14):1935–1954. https://doi.org/10.1111/mice.12974
9. Li Z, Lan Y, Lin W (2024) Footbridge damage detection using smartphone-recorded responses of micromobility and convolutional neural networks. Autom. Constr. 166:105587. https://doi.org/10.1016/j.autcon.2024.105587
10. Li Z, Lan Y, Lin W (2023) Indirect damage detection for bridges using sensing and temporarily parked vehicles. Eng. Struct. 291:116459. https://doi.org/10.1016/j.engstruct.2023.116459

11. Yang YB, Chang KC (2009) Extracting the bridge frequencies indirectly from a passing vehicle: parametric study. Eng. Struct. 31(10):2448–2459. https://doi.org/10.1016/j.engstruct.2009.06.001
12. Shi Z, Uddin N (2021) Extracting multiple bridge frequencies from test vehicle – a theoretical study. J. Sound Vib. 490:115735. https://doi.org/10.1016/j.jsv.2020.115735
13. Kong X, Cai CS, Deng L, Zhang W (2017) Using dynamic responses of moving vehicles to extract bridge modal properties of a field bridge. J. Bridge Eng. 22(6):4017018. https://doi.org/10.1061/(ASCE)BE.1943-5592.0001038
14. Jian X, Xia Y, Sun L (2020) An indirect method for bridge mode shapes identification based on wavelet analysis. Struct. Control Health Monit. 27(12):e2630–e2630. https://doi.org/10.1002/stc.2630
15. Li Z, Lin W, Zhang Y (2023) Bridge frequency scanning using the contact-point response of an instrumented 3D vehicle: theory and numerical simulation. Struct. Control Health Monit. 2023:1–23. https://doi.org/10.1155/2023/3924349
16. Yang YB, Liu YH, Xu H, Guo DZ, Zhou ZY (2024) Unified theory for identifying vertical and radial damping ratios of curved bridges by two connected scanning vehicles. Eng. Struct. 315:118356. https://doi.org/10.1016/j.engstruct.2024.118356
17. Li Z, Lin W, Zhang Y (2023) Drive-by bridge damage detection using Mel-frequency cepstral coefficients and support vector machine. Struct. Health Monit. 22(5):3302–3319. https://doi.org/10.1177/14759217221150932
18. Lan Y, Li Z, Koski K, Fülöp L, Tirkkonen T, Lin W (2023) Bridge frequency identification in city bus monitoring: a coherence-PPI algorithm. Eng. Struct. 296:116913. https://doi.org/10.1016/j.engstruct.2023.116913
19. Cantero D, Hester D, Brownjohn J (2017) Evolution of bridge frequencies and modes of vibration during truck passage. Eng. Struct. 152:452–464. https://doi.org/10.1016/j.engstruct.2017.09.039
20. Yang YB, Cheng MC, Chang KC (2013) Frequency variation in vehicle–bridge interaction systems. Int. J. Str. Stab. Dyn. 13(02):1350019. https://doi.org/10.1142/S0219455413500193
21. Li J, Zhu X, Law S, Samali B (2020) Time-varying characteristics of bridges under the passage of vehicles using synchroextracting transform. Mech. Syst. Signal Process. 140:106727. https://doi.org/10.1016/j.ymssp.2020.106727
22. Tan C, Zhao H, Obrien EJ, Uddin N, Kim C-W (2023) Exploring time-varying characteristics in drive-by bridge frequency extraction with the second-order synchrosqueezing transform. J. Bridge Eng. 28(4):4023010–4023010. https://doi.org/10.1061/JBENF2.BEENG-5979
23. He Y, Yang JP, Yan Z (2023) Estimating modal scale factors based on vehicle-induced variation of bridge frequencies. Eng. Struct. 277:115424. https://doi.org/10.1016/j.engstruct.2022.115424
24. He Y, Yang JP (2022) Using acceleration residual spectrum from single two-axle vehicle at contact points to extract bridge frequencies. Eng. Struct. 266:114538. https://doi.org/10.1016/j.engstruct.2022.114538
25. Li Z, Lan Y, Feng K, Lin W (2024) Investigation of time-varying frequencies of two-axle vehicles and bridges during interaction using drive-by methods and improved multisynchrosqueezing transform. Mech. Syst. Signal Process. 220:111677. https://doi.org/10.1016/j.ymssp.2024.111677
26. Yu G (2021) A multisynchrosqueezing-based high-resolution time-frequency analysis tool for the analysis of non-stationary signals. J. Sound Vib. 492:115813. https://doi.org/10.1016/j.jsv.2020.115813
27. Carmona RA, Hwang WL, Torresani B (1997) Characterization of signals by the ridges of their wavelet transforms. IEEE Trans. Signal Process. 45(10):2586–2590. https://doi.org/10.1109/78.640725

28. Pham D-H, Meignen S (2017) High-order synchrosqueezing transform for multicomponent signals analysis—with an application to gravitational-wave signal. IEEE Trans. Signal Process. 65(12):3168–3178. https://doi.org/10.1109/TSP.2017.2686355